Journal of Molecular Structure 1285 (2023) 135468

Contents lists available at ScienceDirect

Journal of Molecular Structure

journal homepage: www.elsevier.com/locate/molstr

Structural studies of a novel tautomeric Schiff base derived from 4-(*N,N'*-diethylamino)salicylaldehyde and 2-amino-4-methyl phenol: An experimental and theoretical study

S. Asha[a], Anup Thomas[b], S. Suma[a,*], Retheesh K[c], K.S. Sandhya[d], B. Siddlingeshwar[e], M.R. Sudarsanakumar[f]

[a] Department of Chemistry, Sree Narayana College, Chempazhanthy, Research Centre, University of Kerala, Thiruvananthapuram 695587, India
[b] Centre for Computational Research in Clean Energy Technologies, Sree Chitra Thirunal College of Engineering, Trivandrum, India
[c] Department of Chemistry, Government College Kariavattom, Thiruvananthapuram 695481, India
[d] Department of Computational Biology and Bioinformatics, University of Kerala, Thiruvananthapuram 695587, India
[e] Department of Physics, M.S. Ramaiah Institute of Technology, (Autonomous Institute affiliated to VTU) Bengaluru 560054, India
[f] Department of Chemistry, Mahatma Gandhi College, Thiruvananthapuram 695004, India

ARTICLE INFO

Article history:
Received 28 December 2022
Revised 19 March 2023
Accepted 29 March 2023
Available online 30 March 2023

Keywords:
Single crystal X-ray diffraction
Enol-imine (EI) ⇄ keto-amine (KA) tautomerism
DFT
TD-FT
Excited state intramolecular proton transfer (ESIPT), charge transfer (CT) and NLO

ABSTRACT

A novel Schiff base, LMAP synthesized from 4-(*N,N'*-diethylamino)salicylaldehyde and 2-amino-4-methyl phenol has been characterized by single crystal X-ray diffraction and spectroscopic methods. DFT methods is used to investigate the enol-imine (EI) ⇄ keto-amine (KA) tautomeric behavior with respect to phase and in solvent media. The synthesized Schiff base crystallizes in the keto-amine (KA) form in the orthorhombic lattice and Pna21space group with four atoms per unit cell ($Z = 4$). Bond length analysis indicates that the KA form possesses significant zwitter ionic character. Study of electronic absorption and emission properties was conducted in the solid state as well as in different solvents. The UV–Vis result reveals the varied structural preference of the compound depending on the solvent media: polar protic solvents stabilize the KA form, while nonpolar and polar aprotic solvents favor the EI form. Quantum mechanical computations using DFT and TD-DFT also confirm these findings. Fluorescence emission spectra show multiple emission bands which indicate both excited state intramolecular proton transfer (ESIPT) and charge transfer (CT) phenomena occur simultaneously within the molecule. DFT predicted NLO responses of KA and EI were compared and found that the NLO response of KA is superior to that of EI.

1. Introduction

Ortho-hydroxy Schiff bases are an important class of compounds that are of considerable interest to researchers primarily because of their intramolecular hydrogen bonds [1]. These compounds have potential applications in pharmaceutical, computing, and telecommunication [2–5]. They are also highly valued for fabricating microstructures and nanostructures, since they are versatile templates for molecular assembly [6]. Depending on the position of the proton in the H-bond, the ortho-hydroxy Schiff bases exhibit two tautomeric forms: enol-imine (EI) and keto-amine (KA). In the latter case, a proton transfer may bring about a change in the electronic structure, the electronic and protonic states are coupled, thus an intramolecular charge transfer may take place. As a result, a zwitterionic structure may be formed. Scheme 1 represents the tautomeric forms of ortho-hydroxy Schiff base. The tautomer I represents the enol-imine (EI), II the keto-amine (KA) form and III the zwitter ionic form. The structural forms II and III can be regarded as -NH forms. The enol-imine (EI) ⇄ keto-amine (KA) tautomeric equilibrium plays a significant role in many biochemical processes as well [7,8]. The photo-, thermo-, and solvatochromic properties observed in ortho–hydroxy Schiff bases are closely related to EI⇄KA tautomerism [9] and their versatile applications were revealed in both theoretical and experimental investigations [10].

The relative stability of the tautomers depends on the nature and position of substituents on salicylidine or amine groups in addition to external factors such as the nature of the solvent, pH and temperature. The type of substituent on the salicylidine ring affects the electron distribution in the molecule and hence the position of EI/KA equilibrium. The electron-donating substituents at ortho

* Corresponding author.
E-mail address: sumasncw@gmail.com (S. Suma).

https://doi.org/10.1016/j.molstruc.2023.135468
0022-2860/

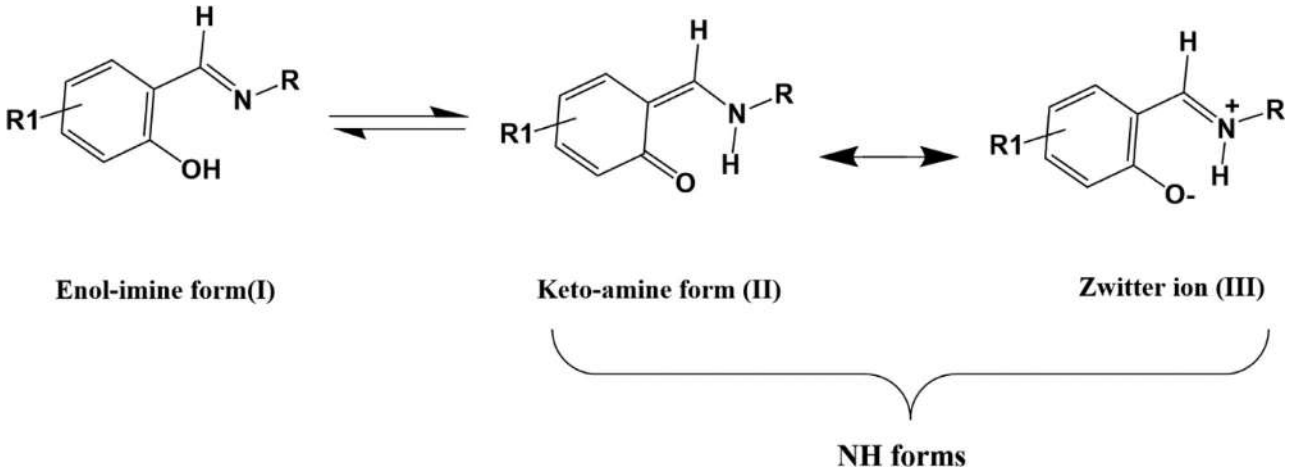

Scheme 1. Enol-imine (EI) / keto-amine (KA) tautomerisation in ortho-hydroxy Schiff base.

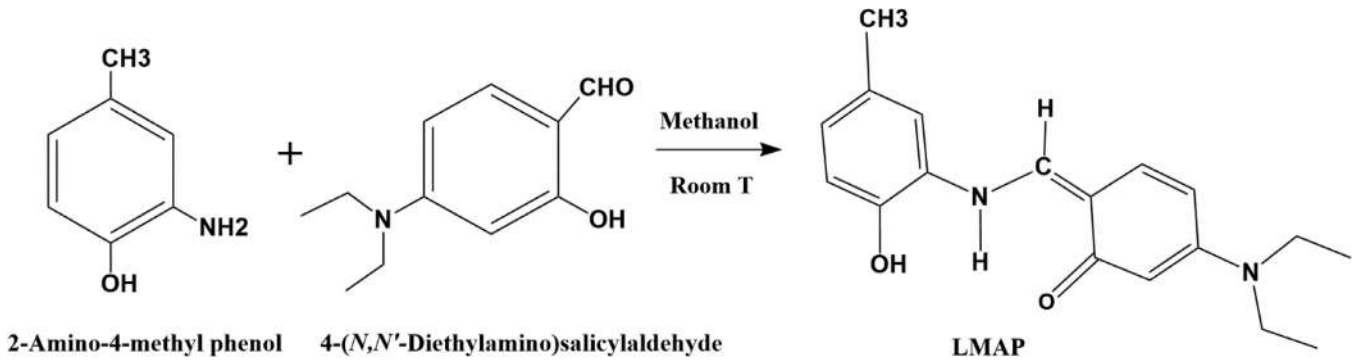

Scheme 2. Synthesis of LMAP.

or para positions with respect to the aldimine bridge increase the basicity of nitrogen. In contrast, the electron-withdrawing groups in the meta positions increase the acidity of the phenolic groups SI(1). In both cases, equilibrium shifts towards KA form [11]. In most cases, equilibrium shifts towards EI form when N-salicylidine anilines do not have any other functional groups [11,12]. The additional OH groups in the salicylidine and aniline rings that create intermolecular hydrogen bonds may also affect the tautomeric equilibrium. It has been revealed that the presence of vicinal -OH or additional -OH in the aniline ring stabilizes the KA form considerably [11–14].

The present study reports the synthesis and characterization of a novel Schiff base derived from 4-*N,N'*-(diethylamino)salicylaldehyde and 2-amino-4-methyl phenol by experimental and theoretical methods. We investigated the structure preference (enol-imine/keto-amine) of the compound under various solvent conditions, using UV-Vis absorption and TD-DFT/RPA methods. Also, the emission properties in the solid state as well as in solvent media and the theoretical NLO response of the tautomers are examined.

2. Experimental methods

AR grade 4-(*N,N'*-diethylamino)salicylaldehyde and 2-amino-4-methyl phenol were purchased from Merk and used as received. Methanol purchased from Merk was used without distillation.

2.1. Synthetic procedure

The classical method of synthesis of imines involves mixing of equimolar amounts of aldehydes or ketones with primary amines [15]. Scheme 2 shows the procedure for the synthesis of Schiff base, LMAP. A solution of 2-amino-4-methyl phenol (0.6158 g, 5.0 mmol) in 20 mL methanol is added to a methanolic solution of 4-(*N,N'*-diethylamino)salicylaldehyde (0.9662 g, 5.0 mmol in 20 mL). The mixture was stirred well and allowed to stand at room temperature. After about 24 h, dark brown crystals suitable for single crystal X–ray studies were separated. (yield: 73% M.P. 183 ± 2 °C)

2.2. Physical measurements

A Perkin Elmer Spectrometer was used to record the FT-IR spectrum using solid KBr pellets in the range 4000–400 cm^{-1}. The electronic spectra were recorded on a Varian Cary 5000 UV–Visible Spectrophotometer in the range 200–600 nm in different solvents. The NMR spectra were recorded on a Bruker Avance III 400 MHz FT-NMR Spectrometer with TMS as the internal standard in $CDCl_3$ solvent at SAIF, CUSAT, Kochi, India. The solid state ^{13}C NMR spectra were recorded in ECX400-Jeol 400 MHz High Resolution Multinuclear FT-NMR Spectrometer at IISc, Bangalore, India. The fluorescence spectra were recorded in Jobin Yvon fluorimeter at SAIF IIT Madras, Chennai, India.

2.3. X-ray crystallography

The single crystal X-ray diffraction data were collected on a Bruker AXS Kappa Apex II CCD diffractometer equipped with graphite monochromated Mo Kα radiation (λ = 0.71073) at 296 K. Cell refinement and data reduction of the compound were carried out by APEX3/SAINT and SAINT/XPREP respectively [16]. The structure solution was done with SHELXT-2014/5 [17].

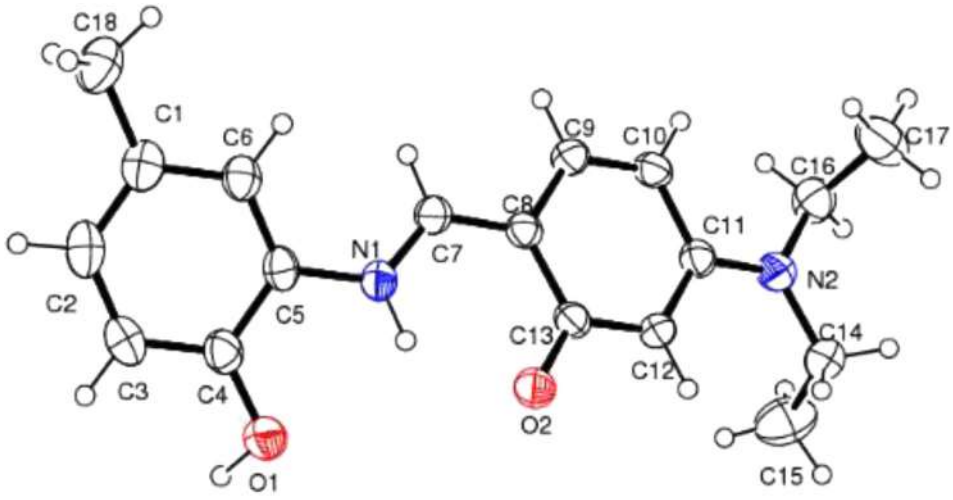

Fig. 1. ORTEP diagram of LMAP with atom numbering.

The structure refinement was carried out with full-matrix least square on F^2 using SHELXL-2018/3 [18]. All non-hydrogen atoms were refined with anisotropic thermal parameters. For structure visualization ORTEP 3 and MERCURY version.3 software were used [19]. Molecular graphics was executed with Mercury software.

2.4. Computational methodology

The geometries of both the tautomeric forms were optimized by wB97XD dispersion corrected range-separated (22% HF exchange at the short range and 100% HF exchange at the long range) version of Becke's 97 density functional and 6–311G(d,p) basis set [20,21]. The calculations are carried out in the gas phase and in n-hexane and methanol solvents. Solvent reaction field effects were accounted using SMD and PCM solvation methodology [22,23]. On the computed geometries, vibrational frequency analysis is performed in order to confirm that the optimized structures have no imaginary frequencies, i.e. they are minimum on the respective potential energy surfaces. In this paper, the TD-DFT/RPA method was employed to determine electronic absorption characteristics. PBE0 was used to predict electronic absorption since it is claimed to be able to provide reasonable estimates of electronic absorption for most organic dyes [24–26]. The Coupled Perturbed Kohn-Sham (CPKS) approach is used to obtain the NLO response parameters [SI(2)]. All the calculations discussed in this work were carried out using G09 electronic simulation package [27].

Table 1
Crystal data and structure refinement details for LMAP.

Empirical formula	C18 H22 N2 O2
Formula weight	298.37
Temperature	296(2) K
Wavelength	1.54178 Å
Crystal system	Orthorhombic
Space group	Pna21
Unit cell dimensions	a = 10.4983(4) Å α= 90° b = 7.0432(3) Å β= 90° c = 21.5030(8) Å γ = 90°
Volume	1589.97(11) Å^3
Z	4
Density (calculated)	1.246 Mg/m3
Absorption coefficient	0.651 mm-1
F(000)	640
Crystal size	0.200 × 0.200 × 0.150 mm3
Theta range for data collection	7.574 to 72.232°
Index ranges	−12<=h<=12, −8<=k<=8, −26<=l<=25
Reflections collected	16718
Independent reflections	3099 [R(int) = 0.0849]
Completeness to theta = 67.679°	99.6%
Absorption correction	Semi-empirical from equivalents
Max. and min. transmission	0.7536 and 0.4703
Refinement method	Full-matrix least-squares on F2
Data / restraints / parameters	3099 / 1 / 211
Goodness-of-fit on F2	1.060
Final R indices [I>2sigma(I)]	R1 = 0.0506, wR2 = 0.1202
R indices (all data)	R1 = 0.0571, wR2 = 0.1246
Absolute structure parameter	−0.11(19)
Extinction coefficient	0.0090(14)
Largest diff. peak and hole	0.165 and −0.171 e. Å-3

3. Result and discussion

3.1. Single crystal X-ray crystallographic structural results

The compound crystallizes in an orthorhombic lattice and space group Pna21with four atoms per unit cell SI(3). An ORTEP view of the asymmetric unit of LMAP is shown in Fig. 1. The single crystal data along with structure refinement details are summarized in Table 1 and the selected geometric parameters are listed in SI(4). The molecule adopts syn conformation with respect to O1 and O2 atoms. The torsion angle for the fragment C(7) –N(1)–C(5)–C(6) (-24.4(5)°) shows that the two rings are not co-planar. The asymmetric unit consists of single molecule in which the hydrogen atom is localized at imine nitrogen (N1H), which indicates that LMAP adopts –NH form at room temperature by the proton assisted EI to KA tautomerization (Fig. 2). The crystallographic evidence for the existence of –NH form of salicylidine Schiff base was first provided by Ogawa et al. [13]. In contrast to the Schiff base compound I (Fig. 3) reported by Ogawa et al., which crystallized in –NH form at 15 K, but shows unresolvable disorder between the –NH and –OH form above 90 K, the crystal structure of the LMAP shows that, the –NH form is more stable at 296 K which is evident from the bond lengths of the N(1)–C(7)–C(8)–C(13) fragment.

For crystallographic assignment of tautomeric forms of salicylidine Schiff bases, the geometric parameters generally followed are:

(**1**) The C(7)–N(1) and C(13)–O(2) bond lengths should be close to double (1.222 Å) and single (1.362 Å) for EI and vice versa for KA forms. (**2**) Comparison of bond lengths of C(8) – C(7) and C(8) – C(13): dC(8) – C(13) > dC(8) – C(7) in KA form and dC(8) – C(13) < dC(8) – C(7) in EI form. (**3**) Generally, the bond length of the C-C bonds of the salicylaldehyde ring has nearly the same

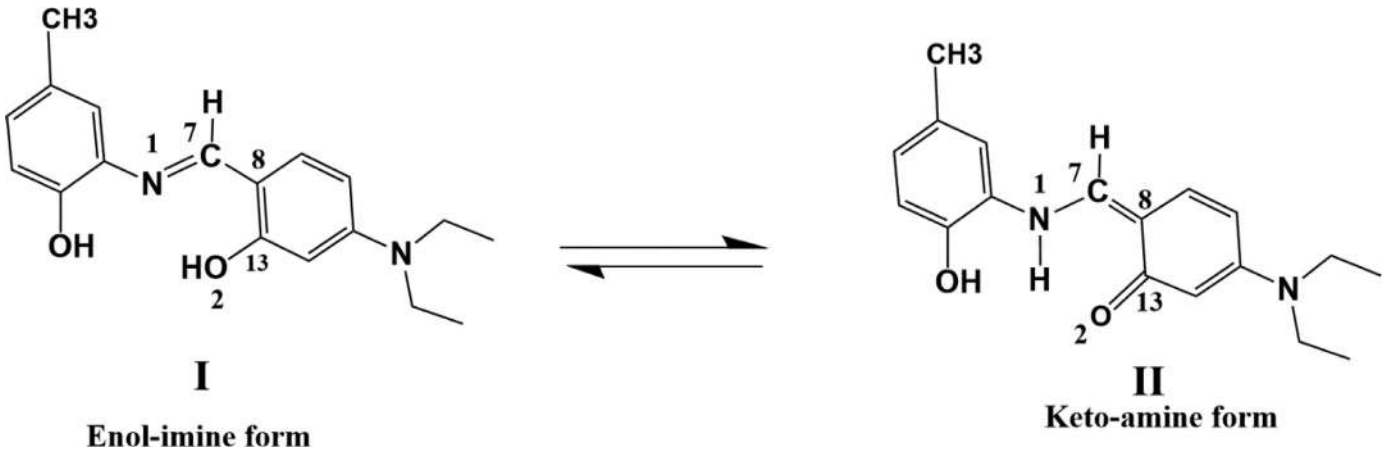

Fig. 2. Enol-imine ⇄ keto-amine tautomerization in LMAP.

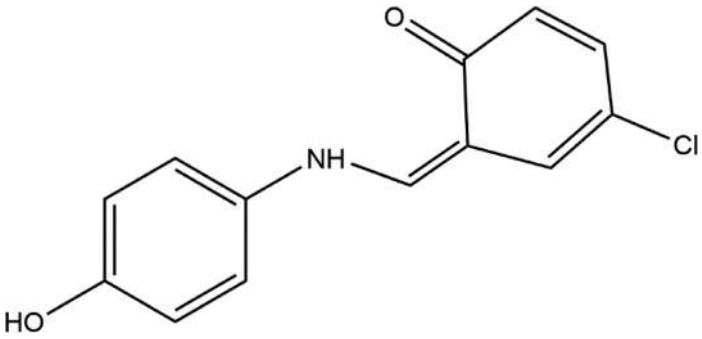

Fig. 3. Chemical structure of the compound I reported as –NH form by Ogawa et al.

value in the EI form (an indication of aromaticity), whereas the KA form has alternate double and single bonds (deviation from aromaticity). Analysis of bond lengths reveals that the O(2) – C(13) bond (1.292 Å) is considerably longer than the C=O bond in conjugate enones (1.222 Å), but shorter than the C–O bonds in phenols (1.362 Å), and the C(7) – N(1) bond length (1.321 Å) shorter than the Csp^2 – N single bond of enamines (1.355 Å) but considerably larger than the Csp^2 =*N* in imines (1.279 Å) [28]. Hence according to criteria 1, these two bonds have an intermediate character. Similarly the C(8) – C(13) bond distance (1.439 Å) is shorter than the C–C single bond (1.464 Å) in conjugated enones, the C(8) – C(7) bond length of 1.384 Å is larger than the Csp^2=C (1.34 Å) in conjugated enones, which satisfies criteria 2 of KA form. These bond lengths are in good agreement with the –NH form of salicylidene Schiff base reported by Ogawa and Harada [13]. The C–C bond lengths of salicylyl ring show significantly longer C8 – C13, C8 – C9, and C10 – C11 bonds (1.439(4), 1.416(5) and 1.426(5) Å) and the shorter C9 – C10 (1.350(5) Å) bond distance (deviation from aromaticity) which is the characteristic of –NH form according to criteria 3. Additionally, the N–H distance of 0.911 Å is close to those reported for Schiff bases which are crystallized in –NH form [11]. Another significant feature of the bond length is the C11 – N2 distance of 1.369 Å, considerably smaller than that of C5 – N1 (1.418 Å) which indicates appreciable double bond character. The shortening and elongation of some of these bonds can be explained only if it is supposed that the KA form of the compound is stabilized by resonance with its canonical zwitter ionic form (III) in which the diethyl amino nitrogen carries a positive charge (Fig. 4). Thus, the stability of the -NH form of LMAP at 296 K in comparison to the compound I (Fig. 3) reported by Ogawa et al., is attributed to the additional resonance stabilization provided by the Et_2N- group in the salicylyl ring. The observed bond lengths of the fragment O(2) – C(13) – C(12) – C(11) – N(2) indicate electronic delocalization along the bonds.

Table 2
Hydrogen bond parameters for LMAP [Å and °].

D–H···A	d(D–H)	d(H···A)	d(D···A)	<(DHA)
N(1)–H(1A)···O(2)	0.91(4)	1.93(4)	2.643(4)	134(3)
O(1)–H(1B)···O(2)#1	1.04(6)	1.56(6)	2.597(4)	171(6)

Symmetry transformations used to generate equivalent atoms:
#1 x+1/2,-y+3/2,z

Both intramolecular and intermolecular hydrogen bond interactions stabilize the crystal structure in which the salicylyl oxygen atom forms bifurcated hydrogen bonds. Table 2 contains the hydrogen bond parameters for LMAP. The intramolecular N – H···O hydrogen bond formed between N(1)H and O(2) [N(1)···O(2) = 2.643(4) Å, H(1)···O(2) = 1.93(4) Å and <N1–H1–O2 = 134° (3)] forms a six membered ring S6 (Fig. 5). As shown in Fig. 5, each molecule acts as a hydrogen donor to one neighboring molecule and an acceptor to another. The hydrogen bond interactions between the amino moiety of one molecule and the salicylidine fragment of neighboring molecule, O(1) – H(1B)···O(2) interactions [O(1)···O(2) = 2.597(4) Å, H(1)···O(2) =1.56(6) Å and <O(1)-H(1)···O(2) = 171(6)°] lead to the formation of hydrogen bonded chain $C_1^1(9)$ and the van der Waals interactions connect these chains into layers. SI(5) shows the crystal packing viewed along the crystallographic axis 'b'. The $\pi-\pi$ interactions between salicyl (C8/C13) and aniline (C1/C6) rings of the adjacent molecules reinforce the crystal packing [SI(6)]. It is interesting to note that the intermolecular hydrogen bond distance [1.56(6) Å] is considerably shorter than that of the intramolecular hydrogen bond [1.93(4) Å], which indicates stronger interaction

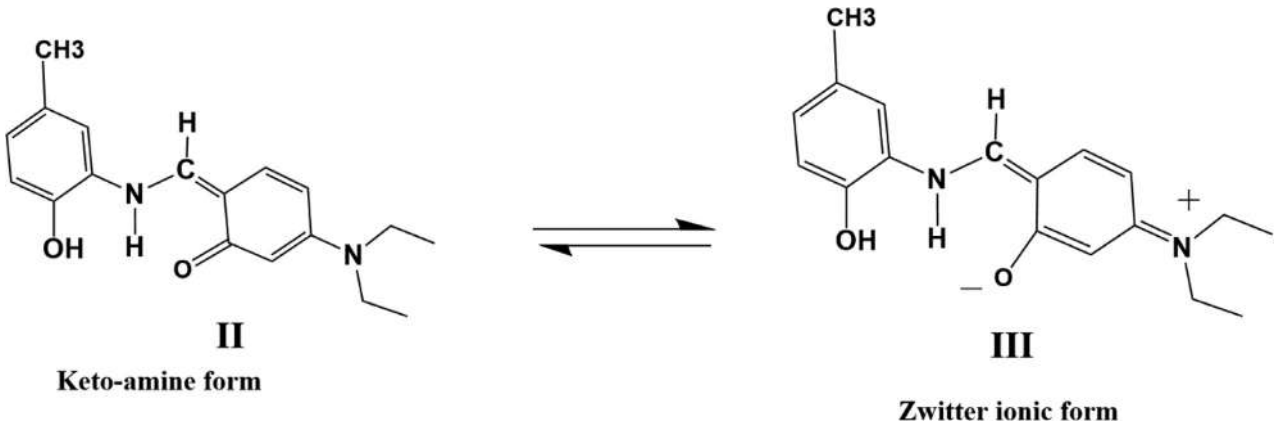

Fig. 4. Stabilization of keto-amine(KA) form II of LMAP with its zwitter ionic form III.

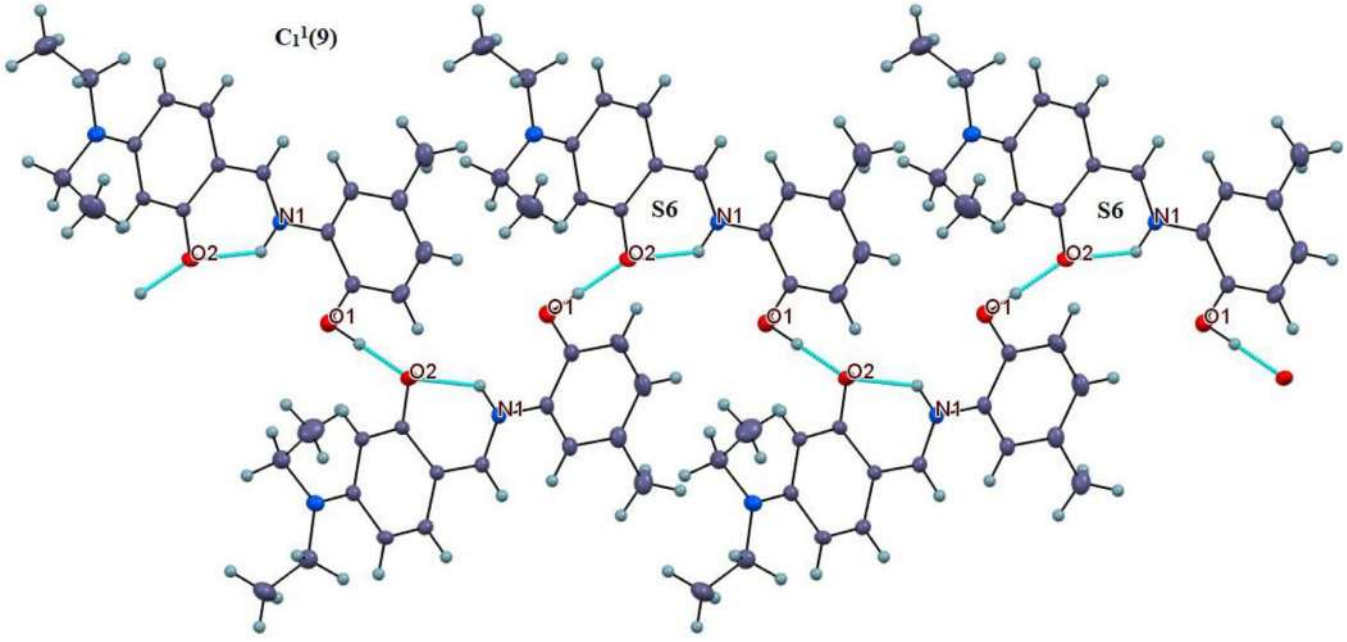

Fig. 5. Hydrogen bonded chains of LMAP.

between molecules. This may be due to the enhanced polarity of the molecule in the zwitter ionic form (III), which may result in strong electrostatic interactions between molecules, thus strengthening the hydrogen bond [14].

The structural change in tautomeric Schiff base can be analyzed by calculating its Harmonic Oscillator model of aromaticity (HOMA) index [29–31]. The HOMA index is the geometrical criterion of local aromaticity, defined as a normalized sum of squares of deviations of bond lengths from the optimal value. It can be calculated using the following equation.

$$HOMA = 1 - \left\{ \frac{\alpha}{n} \sum_{i=1}^{n} (\mathrm{Ri} - \mathrm{Ropt})2 \right\}$$

Where n is the number of bonds in the ring. Ropt =1.388 Å for C - C bond. A fully aromatic system has a HOMA index of 1. We calculated the HOMA index for the C1/C6 and C8/C13 ring as 0.99 and 0.72 respectively, which shows a considerable loss of aromaticity of the C8/13 ring. This is in accordance with those expected for compounds with – NH structural form as a result of deformation of π electron delocalization. Therefore, this result supports the – NH tautomeric form of LMAP as revealed by single crystal X-ray diffraction data.

3.2. ^{1}H NMR spectral studies

Tautomeric Schiff bases can be characterized by NMR spectroscopy. It is expected that the ^{1}H NMR spectrum of the EI form of Schiff base will display a sharp singlet for the imine proton (-CH=N), while the corresponding proton in the KA form will display a doublet due to spin coupling with the amino hydrogen atom. The compound LMAP showed a sharp singlet at 8.392 ppm in $CDCl_3$, which is characteristic of an imine proton [11]. The signals from 7.173 to 6.171 ppm indicate aromatic protons, and the quartet in the region 3.42 to 3.37 ppm indicates methylene protons on C14 and C16. A singlet at 2.30 ppm corresponds to methyl protons on C18, while a triplet corresponding to methyl protons on C15 and C17 is located in the region 1.22 and 1.18 ppm. The two -OH protons present in the molecule which are involved in hydrogen bonding (as revealed by SXRD) do not appear in the spectrum. This may be due to proton exchange with residual water in the solvent. No signal corresponding to the KA form is detected in the $CDCl_3$

solvent, indicating that the equilibrium has shifted towards the EI form (SI(7)).

3.3. ^{13}C NMR spectrum

The chemical shift associated with the carbon bearing keto/enol functionality (here C(13)) is the most sensitive indicator of the predominant tautomeric form in solid and solution state. In the EI tautomer, the C(13) carbon is expected to give a sharp signal around 160 ppm, whereas in the KA form, it shifts towards 180 ppm [32]. SI(8) and SI(9) show the ^{13}C NMR spectra of the LMAP in solid and solution states (in CDCl3) respectively. The solid state ^{13}C NMR spectrum exhibits a sharp signal at 177.47 ppm, which is in good agreement with the reported KA form of similar Schiff bases [33–35]. Absence of signal around 160 ppm indicates the shift of tautomeric equilibrium towards KA form in the solid state. In $CDCl_3$ the compound displayed a sharp signal at 163.97 ppm, indicating the presence of -OH proton at C(13), which indicates a predominant EI form in $CDCl_3$.

3.4. IR spectrum

In the FT-IR spectrum of LMAP SI(10) a broad band is visible around 3450 cm^{-1}, which is a characteristic of uncoordinated OH groups involved in intermolecular hydrogen bonds. When the –OH /–NH groups are not involved in hydrogen bonding, they usually appear as sharp band at higher wave numbers [36]. According to the single crystal X-ray diffraction data the –O(1)H(1) is involved in intermolecular hydrogen bonding with the oxygen atom of the keto group, O(2) [O(1) – H(1)···O(2)], as a consequence of this the corresponding band broadens. Hence the broad band around 3450 cm^{-1} can be assigned to this mode. Crystallographic data revealed that the –NH group is involved in the formation of a six membered ring by intramolecular N(1)–H(1)···O(2) hydrogen bonding. These intramolecular interactions result in a broad -NH band of low intensity towards lower wave numbers [37]. Consequently, the weak broad IR band around 2500 cm^{-1} is assigned to this mode. The band at 1606 cm^{-1} is consistent with the resonance nature of the C=O bond, which supports the zwitterionic nature of the compound. The intense bands at 1236 and 1338 cm^{-1} can be assigned to C–N (single bond) and C_{ar}–N stretching vibrations respectively. The aromatic C–H stretching vibration occurs at 3072 cm^{-1}, the asymmetric and symmetric stretching vibrations of the methyl groups occur at 2969 and 2926 cm^{-1} respectively whereas the corresponding vibrations of methylene group occur at 2888 and 2856 cm^{-1}. The aromatic C–C stretching vibrations appear at 1592, 1523 and 1506 cm^{-1}. The bending vibrations of the methylene group occur at 1475 and 1410 cm^{-1}.

3.5. Electronic spectra

It is possible to identify tautomeric salicylidine Schiff bases by UV–Vis spectroscopy. It has been shown that for EI tautomers, the absorption corresponding to π-π^* transition of imine group (-CH=N) may appear in the range 300–400 nm. On the other hand, the KI form gives a characteristic band of λ_{max}>400 nm due to n-π^* transition of -C=O group. Since solvent polarity and solvent interaction have a marked effect on the EI/KA tautomeric equilibrium [38–42], the absorption spectra of LMAP in different solvents such as n-hexane, chloroform, dichloromethane and methanol were analyzed (Fig. 6). Two major bands were observed in all solvents. The band around 265 nm is attributed to the π-π^* transition of aromatic ring. The second band appears in the region 370–400 nm (except methanol) and corresponds to the π-π^* transition of (-CH=N) group [43]. In methanol, the second band appeared around 424 nm. Since the appearance of a band of λ_{max}>400 nm is a typical characteristic of the KI form [44,45], we can infer that the KI form is largely stabilized in methanol. The stabilization of the KI form in methanol is attributed to the intermolecular hydrogen bonding interaction of the compound with the solvent molecule [46]. Thus, we can conclude that polar protic solvents stabilize the KA tautomer whereas the polar aprotic solvents and the non-polar solvents stabilize the EI form.

3.6. Computational DFT results

(a) On the stability of enol-imine (EI) and keto-amino (KA) tautomeric forms

To get more insight into the experimental observations and corroborate the results we have evaluated the relative stability of each tautomeric form using computational DFT schemes. Together with the gas phase analysis, a study of solvent effects on tautomer stability was also conducted. In n-hexane as well as in methanol, we optimized the structure to compute the energies of the two tautomeric forms. A comparison of two solvent models (IEFPCM and SMD) has been made to determine which solvent model is likely to be most appropriate. We used the DFT functional wB97XD, as well as the basis set 6-311G(d,p) for optimizing the geometries and estimating the energies. Several studies have demonstrated that the wB97XD is a range-separated hybrid functional corrected for dispersion capable of studying the structure, relative stability upon solvation, and estimating the optical properties of tautomers [47–50]. Results of the study are compiled in SI(11)

EI tautomer has better stability in the gas phase by about 4.43 kcal/mol than KA tautomeric form. PCM solvation calculations also predict that the EI tautomer is stabilized over the KA form in either methanol or n-hexane, while experimental evidence favors the KA form in polar aprotic solvents. In line with experimental predictions, the solvation model SMD predicts that the KA tautomer is slightly more stable than the EI form in polar methanol solvent. It may be due to better parameterization and more logical corrections to the cavity, dispersion, and solvent structure effects that are taken into account in SMD formalism. Observing the intramolecular interaction in the experimental crystal geometry, we find that the carbonyl group in the KA form has a strong hydrogen bond with the neighboring molecules' hydroxyl group. With the existing possibility to have hydrogen bonding with the methanol solvent, the stability of KA form may improve in methanol solvation, which can be accurately modeled only by using time consuming explicit solvation and MD simulations.

(b) On the Geometry of enol-imino (EI) and keto-amino (KA) Tautomeric forms

Experimental crystallographic geometric data are only available for the KA form, but little is known about the other participating tautomeric forms. Furthermore, experimental geometric parameters of molecules in solution are not available. This would allow a comparison to be made only if the geometry were computed, which would shed some light on experimentally observed results. This may be approached by optimizing the geometries at a higher DFT level. The geometries are optimized by means of the dispersion corrected range-separated wB97XD/6-311G(d,p) [51,52]. The results are summarized in Fig. 7a and 7b.

For both the PCM and SMD solvation models, the enol O – H bond length in hexane is 0.99 Å, the same value as in the gas phase. When the solvent is changed to more polar Methanol, the bond elongates slightly (0.002 Å). In general, the hydrogen bond distances between enol-H and imine-N decrease as solvent polarity increases. While the hydrogen bond length in KA form (between amino-H and keto-O) increases with increasing solvent polarity.

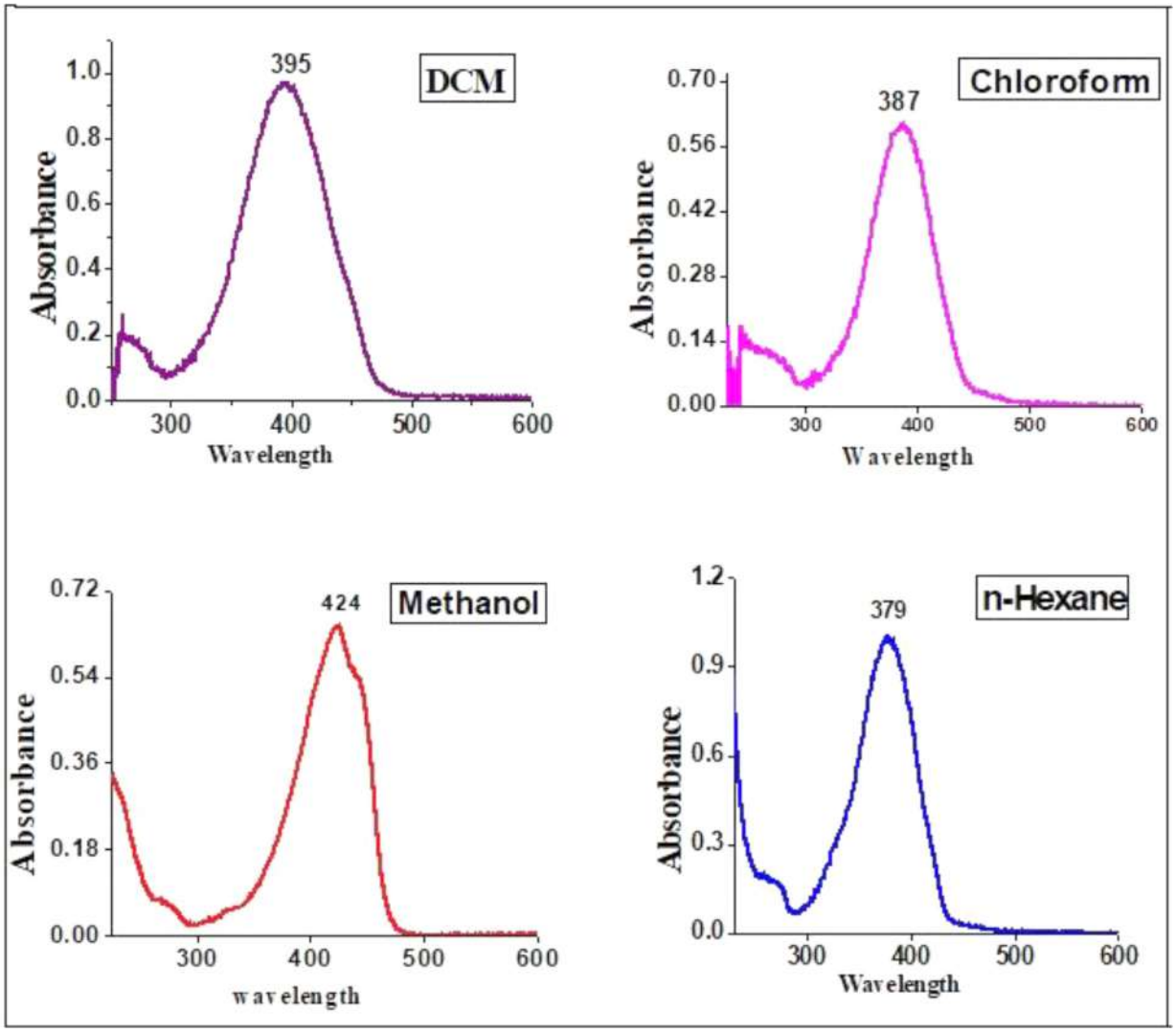

Fig. 6. Electronic spectrum of LMAP in dichloromethane (DCM), Chloroform, methanol and n-Hexane.

Furthermore, there is a trend toward increasing C=O bond length in the KA form from gas-phase (1.249 Å) to hexane (both PCM and SMD 1.253 Å) to methanol (PCM 1.261 Å and SMD 1.269 Å). These are apparently larger than the carbonyl bond lengths of conjugated enones. These data indicate that the C=O bond order is decreased when the solvent assists in hydrogen bonding. The predicted length of C–O bond in EI form is 0.018 Å shorter than that of the normal C–O bond length of Phenol. There is little difference (0.03 Å) between the estimated C–N bond length of the KA form and the C–N bond length found in most enamines, but it is higher than that usually seen in imines (0.05 Å).

(c) On the natural charge obtained from Natural Population Analysis and dipole moment

Additionally, from the natural population analysis, we evaluated each atom's natural charge to explore further insight into the structural details [53] In general, natural populations offer an inexpensive and practical approach to the assessment of covalent and ionic limits. In Fig. 8, we present the results. In the KA form, Hydroxyl-H has a calculated natural charge of 0.510e, while amino-H has a calculated charge of 0.455e. This is because of hydrogen bonds between and within molecules. The carbonyl oxygen atom's charge is greater than the phenolic oxygen atom's charge, while enamine-N possesses a charge about −0.1e larger than amino-N's charge. These results confirm the resonance structure may be close to the zwitterionic form as shown in Fig. 4. We have also computed dipole moments at the same level of theory. Dipole moments of EI form in hexane and methanol are respectively 3.43 D and 3.68 D, while for KA, they are larger, measuring 4.48 D in hexane and 4.75 D in methanol. Therefore, the KA form is more polar and stabilizes in polar solvents much better than EI.

The HOMO and LUMO electron distribution portraits of both tautomers are displayed in Fig. 9, calculated with PBE0/6–311G(d,p). In both tautomeric forms, the molecular orbitals are delocalized across the entire molecular framework. In the Table 3, we present the estimated HOMO and LUMO eigenvalues, the corresponding HOMO-LUMO gaps (HLG) and the S_0-S_1 excitation energies obtained via quantum mechanical simulations using DFT and TDDFT. These values are estimated using DFT functional PBE0 coupled with Pople's split valence 6-311G(d,p) basis set. Stabilization of HOMO and LUMO occurs upon solvation of both tautomeric forms, but changing the polarity does not affect the magnitude of HOMO and LUMO eigenvalues. It is calculated that the HLG of the KA form is lower by approximately 0.25 eV than that of the EI form. In KA form, the frontier orbital distribution differs slightly from that in EI form, with relatively more electron density in the diethylamino region. In addition, KA form has a relatively low HLG, resulting in better intramolecu-

Table 3
The HOMO, LUMO eigenvalues, HLG and electronic absorption energies, corresponding oscillatory strength as well as orbital contribution of corresponding electronic transitions calculated at wB97XD//TD-PBE0 DFT.

		HOMO	LUMO	HLG	$\Delta E(S_0\text{-}S_1)$ eV[a]	*f*	Orbital contributions
EI	(in Vacuo)	-5.36	-1.12	4.24	3.66	0.951	H→L (93 %)
	(in Hexane)	-5.44	-1.28	4.16	3.53	1.134	H→L (95 %)
	(in Methanol)	-5.44	-1.30	4.14	3.52	1.130	H→L (95 %)
KA	(in Vacuo)	-5.31	-1.48	3.83	3.15 3.46	0.070 0.369	H→L (83 %)
	(in Hexane)	-5.54	-1.64	3.90	3.25 3.38	0.336 0.910	H→L (46 %) H-1→L (53 %)
	(in Methanol)	-5.54	-1.67	3.87	3.20 3.35	0.213 1.048	H→L (38 %) H-1→L (61 %)

lar charge transfer, thereby reducing one-photon absorption energy (redshift).

Due to the experimental fact that the KA form predominated in polar protic solvents, while the EI form predominated in polar aprotic and nonpolar solvents, we thought to complement the observation with TD-DFT calculations to better understand the electronic absorption characteristics of both tautomeric forms. Based on the wB97XD/6-311G(d,p) optimized ground state structure, electronic absorption features of both tautomeric forms were also calculated using single point TD-DFT calculations (PBE0/6311G(d,p)). TD-DFT calculations were also performed in hexane and methanol solvents using the PCM model. In the same Table 3, absorption energies, oscillatory strength, and orbital contributions are summarized. The calculated absorption energy indicates that solvent polarity has little effect on the wavelength of maximum absorption (λ_{max}). As compared to EI forms, KA forms absorb at a longer wavelength of about 30 to 35 nm. In addition, it is interesting to note that the KA form has an intense dipole allowed electronic transition at a shorter wavelength approximately 15 to 20 nm lower than the first absorption shoulder peak. It is exactly in accordance with the experimental UV–Vis absorption spectral features recorded in methanol. Furthermore, in aprotic solvents such as n-hexane, no band associated with KA forms appears. It can be concluded from these observa-

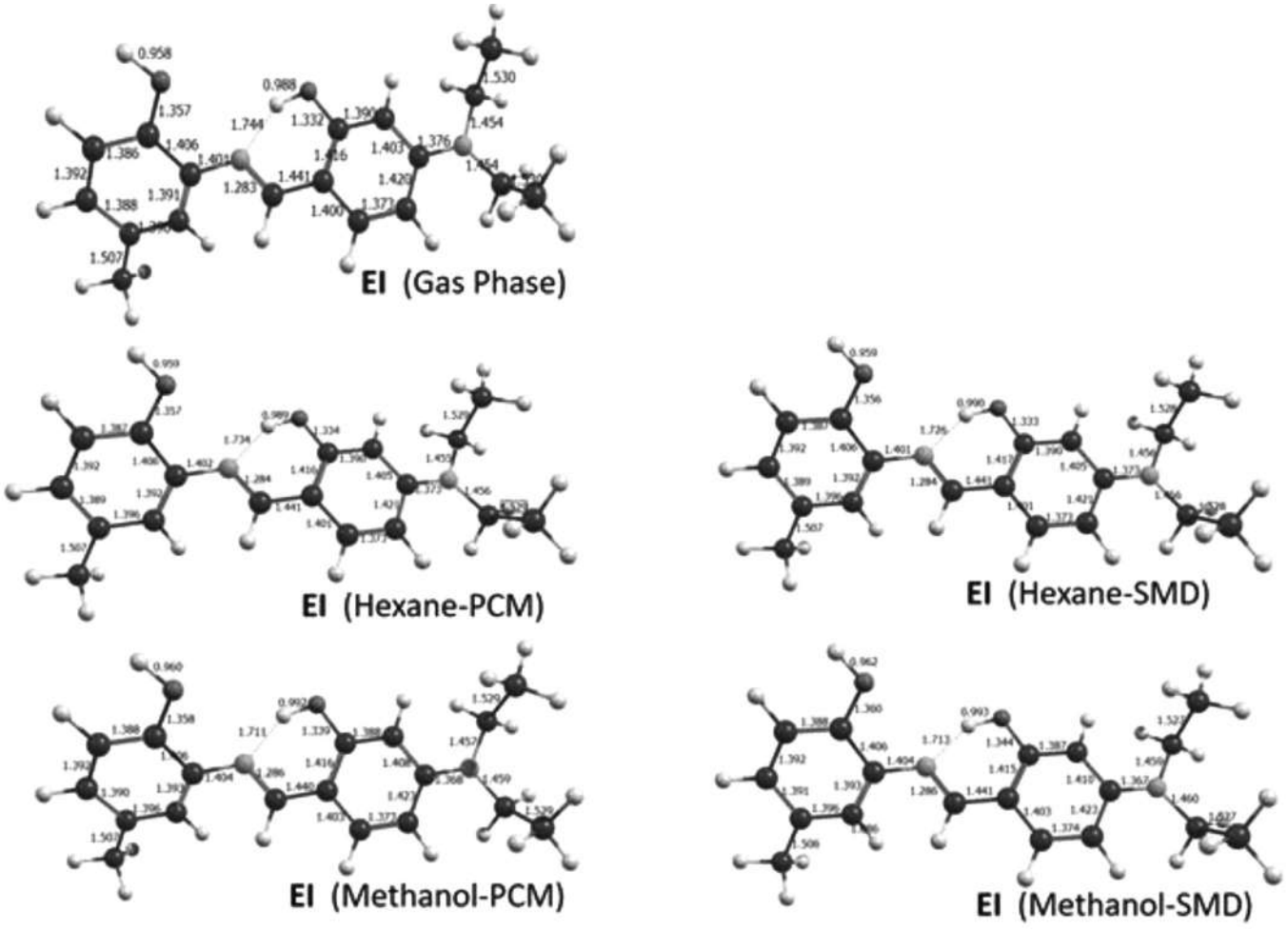

Fig. 7. (a). The optimized geometries of EI form obtained in Gas phase, and in Hexane and methanol Solvents. (b): The optimized geometries with the bond lengths of KA form obtained in Gas phase, and in Hexane and methanol solvents.

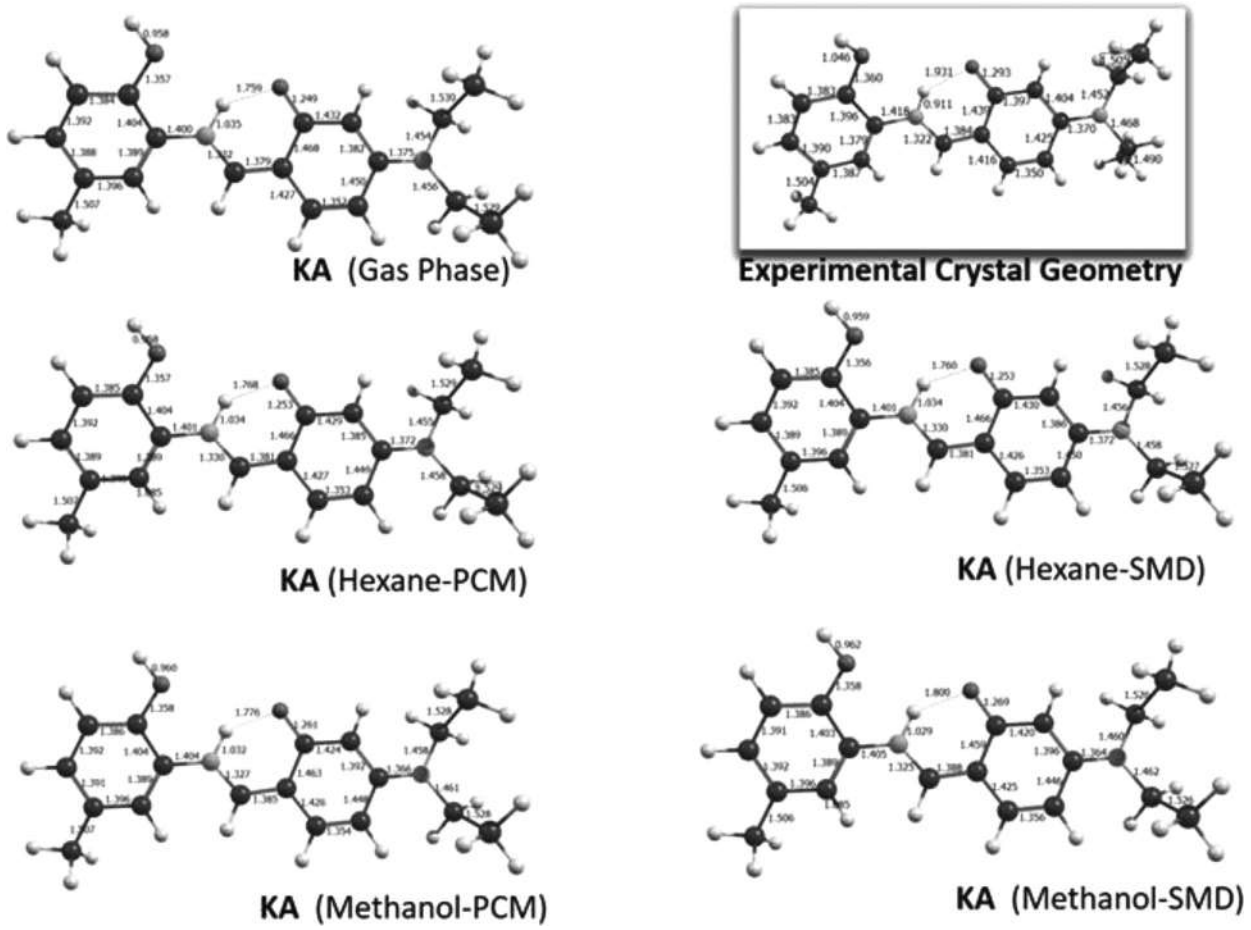

Fig. 7. Continued

Table 4
Isotropic (<α>) and anisotropic ($\Delta\alpha$) mean polarizabilities, first (β) and second (γ) hyperpolarizabilities obtained using Lc-BLYP/6–31+G(d,p)

	<α>[a]	$\Delta\alpha$[a]	$\beta(0)$[b]	β(EOPE)[b]	β(SHG)[b]	$\gamma(0)$[c]	γ(EOKE)[c]	γ(SHG)[c]
Keto-Amine (KA) form (in methanol)	62.93	91.26	31.75	49.59	997.99	386.02	1237.94	42,313.5
Enol-Imine (EI form) (in Hexane)	56.46	70.56	32.90	90.65	231.17	198.32	725.85	1436.43

[a] Dynamic mean polarizabilities (ω 532 nm), value x 10^{-24}esu.
[b] value x 10^{-30}esu.
[c] value x 10^{-36}esu.

tions that pure KA tautomer exists only in protic solvents, such as methanol.

(d) DFT estimated NLO response

Based on our observations of polar solvents favoring the KA form, and nonpolar solvents favoring the EI form, it seemed ideal to estimate the molecular level NLO parameters for both. In this study, we calculated the static and dynamic (laser frequency 532 nm) mean values of polarizability (α), first hyperpolarizability (β) and second hyperpolarizability (γ) using LC-BLYP DFT functional coupled with Pople's split valence basis set (6–311 ++ g(d,p)), which has proven reliable in numerous studies of organic π-conjugated molecules [54–60]. Table 4 presents the results of the study, where the values of NLO parameters are calculated as described in a large number of publications (see SI(2) for equations). Integral equation formalism (IEF-PCM) was also used to account for solvation effects. The table contains the dynamic isotropic and anisotropic polarizabilities (<α>, $\Delta\alpha$), the static β(0, 0, 0), frequency-dependent β(-ω, ω, 0) the electro-optic Pockel's effect (EOPE) as well as β(-2ω, ω, ω) the second harmonic generation (SHG), static γ (0, 0, 0,0), γ(-ω, ω,0,0) associated with electro-optic Kerr effect (EOKE), and γ(-2ω,ω,ω,0) the electric field induced SHG. In this discussion, the values are expressed in esu and the reported magnitudes α, the values need to be multiplied by 10-24, for β by 10-30, and for γ by 10-36.

We will begin by discussing dipole polarizabilities, which are measures of electron cloud distortions when exposed to a weak electric field. There is only a slight difference between the isotropic polarizabilities of the two forms; however, the anisotropic polarizability of the KA form is almost 1.3 times greater. Both forms are predicted to have nearly identical static β, but the dynamic β differs greatly. For the KA form, (EOPE) is nearly twice as good and the (SHG) is almost 4.3 times better than EI. The estimated γ values also indicate a fairly better NLO response for KA than for EI, as well.

3.7. Emission studies

We have examined the fluorescence emission characteristics of LMAP in different solvents as well as those of crystalline

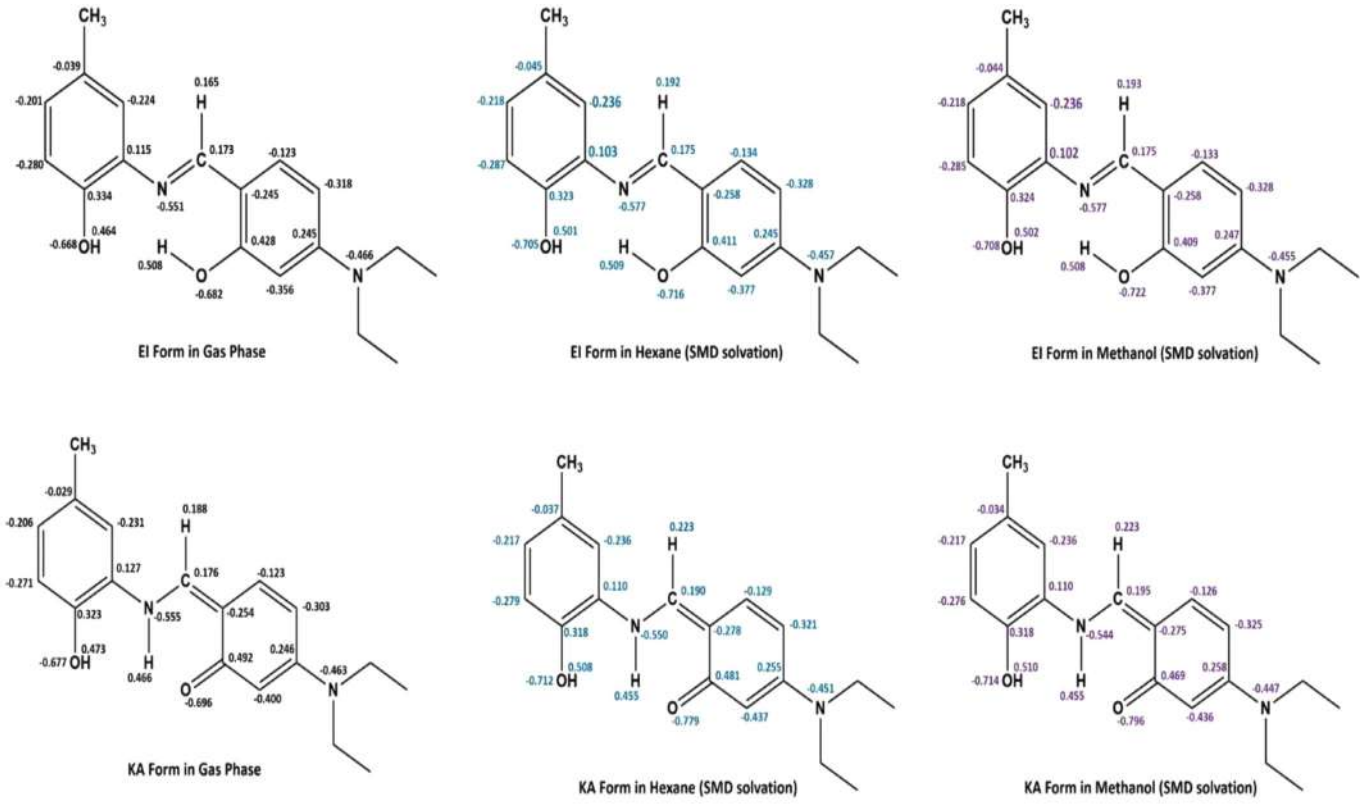

Fig. 8. The natural atomic charges obtained from the NBO calculation using wB97XD/6–311G(d,p) model chemistry.

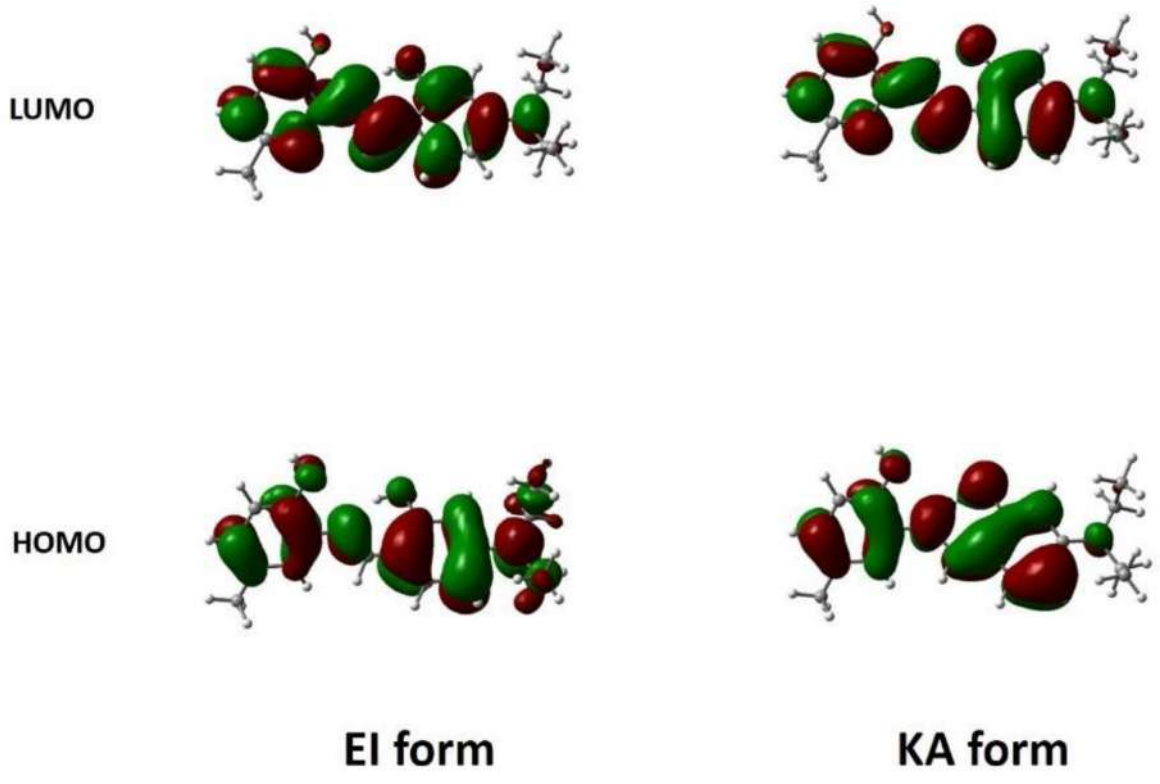

Fig. 9. The frontier molecular orbital picture of EI and KA tautomeric forms obtained using PBE0/6–311G(d,p).

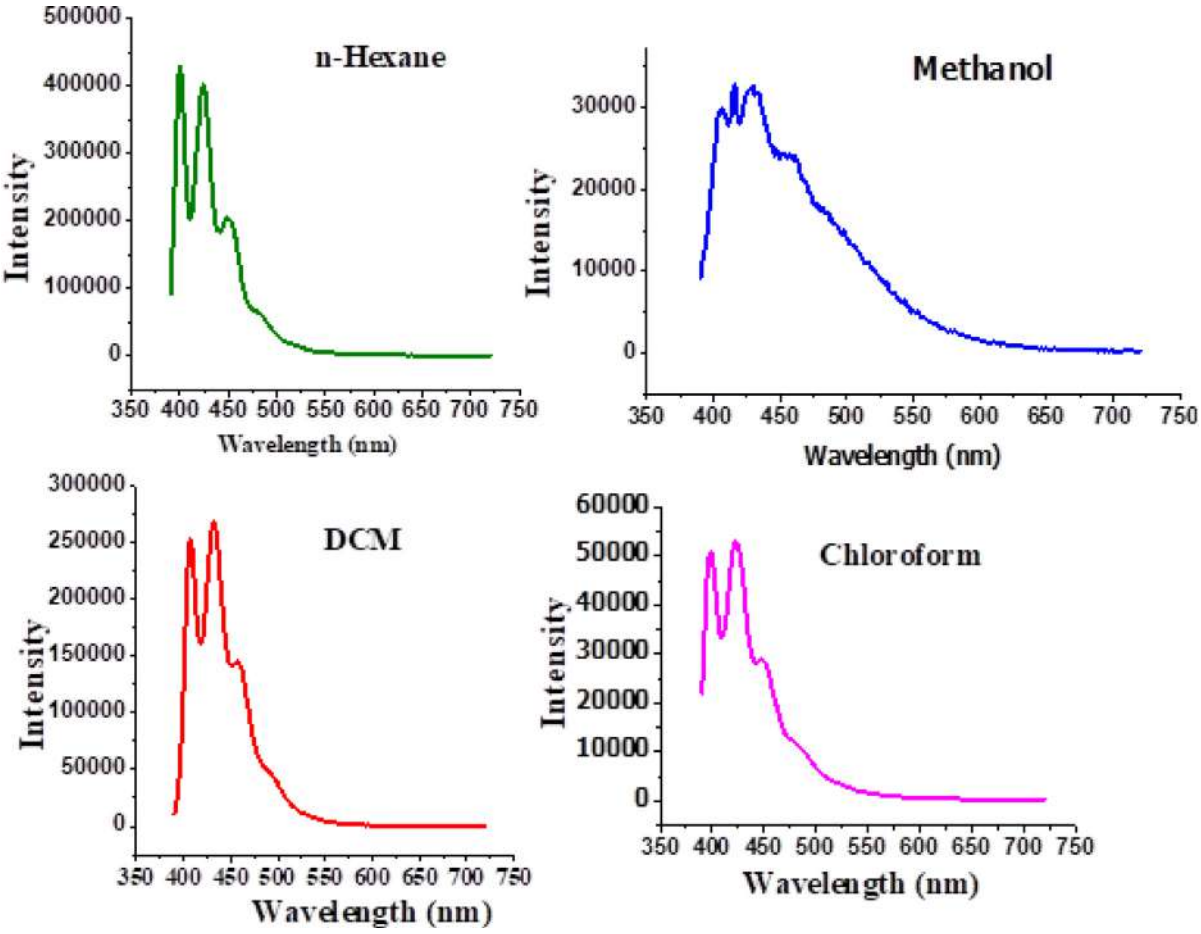

Fig. 10. Emission spectra of LMAP in different solvents.

and powder forms. We observed four bands in aprotic and non-polarsolvent. In n-hexane solvent, the maxima are at 399, 424, 449, and 482 nm, with the last two bands being shoulders (Fig. 10). Two of the bands are local emission (LE) of two tautomeric forms, and the remaining two bands are twisted intramolecular charge transfer TICT [61]. Similar observations are seen for chloroform and dichloromethane solvents. It is clear that the spectrum represents a superposition of fluorescence spectra from the two tautomeric (EI ⇄ KA) forms. Due to the absence of dual absorption and the multiple emission bands, it is evident that excited state intramolecular proton transfer (ESIPT) results in the other tautomer form. The emission spectrum of LMAP in polar protic solvent, methanol shows an additional fluorescence maximum at 416 nm. The KA form is also present in methanol, so this emission may be from one of its rotameric species. The emission intensity is high in non-polar media and in polar-protic solvent, the intensity decreases. In polar solvents, intermolecular hydrogen bonding is formed with the keto/enol form. Hence, the photo-induced charge transfer process is hindered, and the fluorescence intensity decreases [62]. Contrary to this, the emission spectra of solids only showed ICT emission at 547 nm (of crystals) and 522 nm (of powders) (Fig. 11). This long wavelength bands are most likely caused by excimer emission.

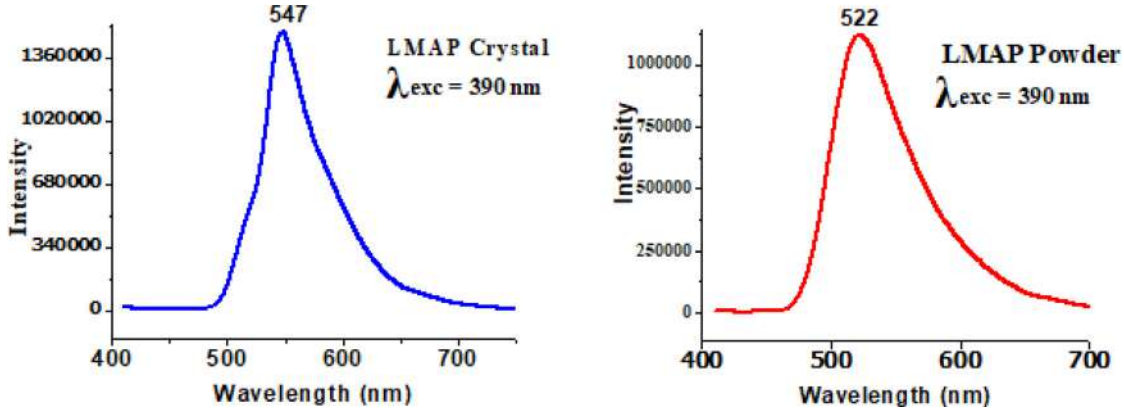

Fig. 11. Emission spectra of LMAP crystal and powder.

Excimer emission is largely quenched in solvents. It is possible to observe mechanical luminescence for LMAP since the emission maxima wavelength differences between powder sample and crystalline sample exceed 25 nm. The red-shift of fluorescence emission in crystal could be due to π–π stacking interaction [63].

4. Conclusion

The synthesis, crystallographic and spectral characterization as well as the DFT studies of enol-imine (EI) ⇄ keto-amine (KA) tautomeric properties of a novel Schiff base are reported. Crystallographic studies reveal that the compound crystallized in the keto-amine (KA) form is resonance stabilized with its zwitter ionic form. The KA form is stabilized by both intra (–N–H···O) and intermolecular (O – H···O) hydrogen bond interactions. Observations by electronic absorption spectra demonstrate that the predominant tautomer in solution is dependent on the solvent media; KA forms in protic solvents and EI forms in aprotic solvents. Computational simulations reveal that the relative energy difference between the two forms is only marginal, with the EI form slightly favored in the gas phase and in nonpolar solvents, whereas the KA form is favored in methanol. The TD-DFT method of electronic absorption spectral studies support the experimental findings. Fluorescence spectra show multiple emission bands that are associated with excited state intramolecular proton transfer (ESIPT) and charge transfer (CT) and the intensity of these bands varies depending on the solvent nature: higher in nonpolar solvents, but decreases in polar-protic solvents. The computationally obtained dynamic NLO responses show that KA has better NLO response than EI. It is expected that the present study will provide useful insights into the design of multi-stimuli-responsive materials.

Supplementary data

CCDC 2045112 contains supplementary crystallographic data for this paper. These data can be obtained free of charge from The Cambridge Crystallographic Data Center via www.ccdc.cam.ac.uk/data_request/cif.

Declaration of Competing Interest

There are no known conflicts of interest associated with this publication.

CRediT authorship contribution statement

S. Asha: Conceptualization, Formal analysis, Methodology, Validation, Writing – original draft, Writing – review & editing. **Anup Thomas:** Conceptualization, Formal analysis, Methodology, Validation, Writing – original draft, Writing – review & editing. **S. Suma:** Supervision, Resources, Writing – review & editing. **Retheesh K:** Conceptualization, Formal analysis, Methodology, Validation, Writing – original draft, Writing – review & editing. **K.S. Sandhya:** Formal analysis, Methodology, Writing – review & editing. **B. Siddlingeshwar:** Conceptualization, Formal analysis, Methodology, Validation, Writing – original draft, Writing – review & editing. **M.R. Sudarsanakumar:** Writing – review & editing.

Data availability

Data will be made available on request.

Acknowledgments

The authors are thankful to the Sophisticated Analytical Instrumentation Facility, STIC, Cochin University of Science and Technology, Kochi, India; SAIF and Indian Institute of Science, Bangalore, India; SAIF, Indian Institute of Technology Madras, India for providing instrumental facilities.

Supplementary materials

Supplementary material associated with this article can be found, in the online version, at doi:10.1016/j.molstruc.2023.135468.

References

[1] A. Filarowski, Intramolecular hydrogen bonding ino-hydroxyaryl Schiff bases, J. Phys. Org. Chem. 18 (8) (2005) 686–698, doi:10.1002/poc.940.
[2] A. Filarowski, A. Koll, L. Sobczyk, Intramolecular hydrogen bonding in o-hydroxy Aryl Schiff bases, Curr. Org. Chem. 13 (2) (2009) 172–193, doi:10.2174/138527209787193765.
[3] K. Amimoto, T. Kawato, Photochromism of organic compounds in the crystal state, J. Photochem. Photobiol. C 6 (4) (2005) 207–226, doi:10.1016/j.jphotochemrev.2005.12.002.
[4] A. Staykov, M. Watanabe, T. Ishihara, K. Yoshizawa, Photoswitching of conductance through salicylidene methylamine, J. Phys. Chem. C 118 (47) (2014) 27539–27548, doi:10.1021/jp5081884.
[5] S. Dalapati, S. Jana, N. Guchhait, Anion recognition by simple chromogenic and chromo-fluorogenic salicylidene Schiff base or reduced-Schiff base receptors, Spectrochim. Acta Part A 129 (2014) 499–508, doi:10.1016/j.saa.2014.03.090.
[6] Y. Jia, J. Li, Molecular assembly of Schiff Base interactions: construction and application, Chem. Rev. 115 (3) (2014) 1597–1621, doi:10.1021/cr400559g.
[7] A.L. Sobolewski, W. Domcke, C. Hattig, Tautomeric selectivity of the excited-state lifetime of guanine/cytosine base pairs: the role of electron-driven proton-transfer processes, Proc. Natl Acad. Sci. 102 (50) (2005) 17903–17906, doi:10.1073/pnas.0504087102.
[8] A. Furmanchuk, O. Isayev, L. Gorb, O.V. Shishkin, D.M. Hovorun, J. Leszczynski, Novel view on the mechanism of water-assisted proton transfer in the DNA bases: bulk water hydration, Phys. Chem. Chem. Phys. 13 (10) (2011) 4311, doi:10.1039/c0cp02177f.
[9] K. Ogawa, J. Harada, T. Fujiwara, S. Yoshida, Thermochromism of salicylideneanilines in solution: aggregation-controlled proton tautomerization, J. Phys. Chem. A 105 (13) (2001) 3425–3427, doi:10.1021/jp003985f.
[10] R. Herzfeld, P. Nagy, Studies of the solvent effect observed in the absorption spectra of certain types of Schiff bases, Curr. Org. Chem. 5 (3) (2001) 373–394, doi:10.2174/1385272013375599.
[11] S.D. Chatziefthimiou, Y.G. Lazarou, E. Hadjoudis, T. Dziembowska, I.M. Mavridis, Keto forms of salicylaldehyde Schiff Bases: structural and theoretical aspects, J. Phys. Chem. B 110 (47) (2006) 23701–23709, doi:10.1021/jp064110p.
[12] V.I. Minkin, A.V. Tsukanov, A.D. Dubonosov, V.A. Bren, Tautomeric Schiff bases: iono-, solvato-, thermo- and photochromism, J. Mol. Struct. 998 (1–3) (2011) 179–191, doi:10.1016/j.molstruc.2011.05.029.
[13] K. Ogawa, Y. Kasahara, Y. Ohtani, J. Harada, Crystal structure change for the thermochromy of N-salicylideneanilines. The first observation by X-ray diffraction, J. Am. Chem. Soc. 120 (28) (1998) 7107–7108, doi:10.1021/ja980972v.
[14] K. Ogawa, J. Harada, I. Tamura, Y. Noda, X-Ray Crystallographic analysis of the NH form of a salicylideneaniline at 15K, Chem. Lett. 29 (5) (2000) 528–529, doi:10.1246/cl.2000.528.
[15] Ed. S. Patai, in: The Chemistry of Carbon-Nitrogen Double Bond, John Wiley and Sons, New York, 1970, pp. 61–146.
[16] Bruker, APEX3, SAINT AND SADABS, Bruker, AXS Inc., Madison, Wisconsin, USA 2016.
[17] G.M. Sheldrick, SHELXT- integrated space-group and crystal-structure determination, Acta Crystallogr. A71 (2015) 3–8.
[18] G.M. Sheldrick, A short history of SHELX, Acta Crystallogr. 64 (Pt.1) (2008) 112–122.
[19] I.J. Bruno, J.C. Cole, P.R. Edgington, M. Kesseler, C.F. Macrae, P.M. Mccabe, J. Pearson, R. Taylor, New software for searching the Cambridge structure database and visualizing crystal structure, Acta Crystallogr. B 58 (2002) 389–397.
[20] C. Halsey-Moore, P. Jena, J.T. McLeskey Jr, Tuning range-separated DFT functionals for modeling the peak absorption of MEH-PPV polymer in various solvents, Comput. Theor. Chem. 1162 (2019) 112506, doi:10.1016/j.comptc.2019.112506.
[21] J.-D. Chai, M. Head-Gordon, Long-range corrected hybrid density functionals with damped atom-atom dispersion corrections, Phys. Chem. Chem. Phys. 10 (2008) 6615–6620, doi:10.1039/b810189b.
[22] A.V. Marenich, C.J. Cramer, D.G. Truhlar, Universal solvation model based on solute electron density and on a continuum model of the solvent defined by the bulk dielectric constant and atomic surface tensions, J. Phys. Chem. B 113 (2009) 6378–6396, doi:10.1021/jp810292n.
[23] J. Tomasi, B. Mennucci, R. Cammi, Quantum mechanical continuum solvation models, Chem. Rev. 105 (2005) 2999–3093, doi:10.1021/cr9904009.
[24] D. Jacquemin, E.A. Perpète, G.E. Scuseria, I. Ciofini, C. Adamo, TD-DFT performance for the visible absorption spectra of organic dyes: conventional versus long-range hybrids, J. Chem. Theory Comput. 4 (2008) 123–135, doi:10.1021/ct700187z.
[25] D. Jacquemin, V. Wathelet, E.A. Perpète, C. Adamo, Extensive TD-DFT benchmark: singlet-excited states of organic molecules, J. Chem. Theory Comput. 5 (2009) 2420–2435, doi:10.1021/ct900298e.

[26] A. Ali, M.I. Rafiq, Z. Zhang, J. Cao, R. Geng, B. Zhou, W. Tang, TD-DFT benchmark for UV-visible spectra of fused-ring electron acceptors using global and range-separated hybrids, Phys. Chem. Chem. Phys. 22 (2020) 7864–7874, doi:10.1039/d0cp00060d.
[27] M.J. Frisch, G.W. Trucks, H.B. Schlegel, G.E. Scuseria, M.A. Robb, J.R. Cheeseman, G. Scalmani, V. Barone, B. Mennucci, G.A. Petersson, H. Nakatsuji, M. Caricato, X. Li, H.P. Hratchian, A.F. Izmaylov, J. Bloino, G. Zheng, J.L. Sonnenberg, M. Hada, M. Ehara, K. Toyota, R. Fukuda, J. Hasegawa, M. Ishida, T. Nakajima, Y. Honda, O. Kitao, H. Nakai, T. Vreven, J.A. Montgomery, J.E. Peralta, F. Ogliaro, M. Bearpark, J.J. Heyd, E. Brothers, K.N. Kudin, V.N. Staroverov, R. Kobayashi, J. Normand, K. Raghavachari, A. Rendell, J.C. Burant, S.S. Iyengar, J. Tomasi, M. Cossi, N. Rega, J.M. Millam, M. Klene, J.E. Knox, J.B. Cross, V. Bakken, C. Adamo, J. Jaramillo, R. Gomperts, R.E. Stratmann, O. Yazyev, A.J. Austin, R. Cammi, C. Pomelli, J.W. Ochterski, R.L. Martin, K. Morokuma, V.G. Zakrzewski, G.A. Voth, P. Salvador, J.J. Dannenberg, S. Dapprich, A.D. Daniels, Ö. Farkas, J.B. Foresman, J.V. Ortiz, J. Cioslowski and D.J. Fox, Gaussian 09,Revision A.1, Gaussian, Inc., Wallingford, CT, 2009.
[28] R. Oketani, H. Takahashi, M. Hoquante, C. Brandel, P. Cardinael, G. Coquerel, NH-form of a threonine-based Schiff base in the solid state, J. Mol. Struct. (2019), doi:10.1016/j.molstruc.2019.01.093.
[29] H. Houjou, H. Shingai, K. Yagi, I. Yoshikawa, K. Araki, Mutual interference between intramolecular proton transfer sites through the adjoining π-conjugated system in Schiff bases of double-headed, fused salicylaldehydes, J. Org. Chem. 78 (18) (2013) 9021–9031, doi:10.1021/jo401108z.
[30] T.M. Krygowski, Crystallographic studies of inter- and intramolecular interactions reflected in aromatic character of. pi. -electron systems, J. Chem. Inf. Model. 33 (1) (1993) 70–78, doi:10.1021/ci00011a011.
[31] A. Filarowski, A. Kochel, M. Kluba, F.S. Kamounah, Structural and aromatic aspects of tautomeric equilibrium in hydroxy aryl Schiff bases, J. Phys. Org. Chem. 21 (11) (2008) 939–944, doi:10.1002/poc.1403.
[32] C.M. Atzin-Macedo, C. Pastor-Ramírez, R. González-Peláez, F.J. Pérez-Flores, S. Hernández-Anzaldo, H. Vazquez-Lima, Y. Reyes-Ortega, Tautomeric study of Schiff bases derived from o -Dihydroxybenzaldehyde by UV–Vis, IR, 1H NMR, 13 C NMR spectroscopy and computational modeling, ChemistrySelect 5 (36) (2020) 11120–11126, doi:10.1002/slct.202002398.
[33] O. Domínguez, B. Rodríguez-Molina, M. Rodríguez, A. Ariza, N. Farfán, R. Santillan, X-Ray crystallographic and spectroscopic properties of eight Schiff bases as evidence of the proton transfer reaction. Role of the intermolecular hydrogen bond, New J. Chem. 35 (1) (2011) 156–164, doi:10.1039/c0nj00179a.
[34] A. Makal, W. Schilf, B. Kamieński, A. Szady-Chelmieniecka, E. Grech, K. Woźniak, Hydrogen bonding in Schiff bases – NMR, structural and experimental charge density studies, Dalton Trans. 40 (2) (2011) 421–430, doi:10.1039/c0dt00298d.
[35] S.R. Salman, J.C. Lindon, R.D. Farrant, T.A. Carpenter, Tautomerism in 2-hydroxy-1-naphthaldehyde schiff bases in solution and the solid state investigated using13C NMR spectroscopy, Magn. Reson. Chem. 31 (11) (1993) 991–994, doi:10.1002/mrc.1260311107.
[36] P. Gilli, V. Bertolasi, V. Ferretti, G. Gilli, J. Am. Chem. Soc. 122 (2000) 10405–10417, doi:10.1021/ja000921.
[37] D. Lin-Vien, N.B. Colthup, W.G. Fately, J.G. Grasselli, Infrared and Raman Characteristic Frequencies of Organic Molecules, Academic Press, Boston, 1991.
[38] S.H. Alarcón, A.C. Olivieri, D. Sanz, R.M. Claramunt, J. Elguero, Substituent and solvent effects on the proton transfer equilibrium in anils and azo derivatives of naphthol. Multinuclear NMR study and theoretical calculations, J. Mol. Struct. 705 (1–3) (2004) 1–9, doi:10.1016/s0022-2860(03)00208-4.
[39] E.N. Shepelenko, A.V. Tsukanov, Y.V. Revinskii, A.D. Dubonosov, V.A. Bren', V.I Minkin, Benzoid-quinoid tautomerism of schiff bases and their structural fg: LIII. Schiff bases derived from 5-hydroxy- and 5-hydroxy-6-nitro-2,3-diphenyl-1-benzofuran-4-carbaldehydes, Russ. J. Org. Chem. 43 (4) (2007) 559–563, doi:10.1134/s1070428007040124.
[40] V.P. Rybalkin, A.D. Dubonosov, E.N. Shepelenko, L.L. Popova, N.I. Makarova, A.V. Tsukanov, … V.I. Minkin, Russ. J. Org. Chem. 38 (9) (2002) 1326–1330, doi:10.1023/a:1021607930539.
[41] M. Yıldız, Z. Kılıç, T. Hökelek, Intramolecular hydrogen bonding and tautomerism in Schiff bases. Part I. Structure of 1,8-di[N-2-oxyphenylsalicylidene]-3,6-dioxaoctane, J. Mol. Struct. 441 (1) (1998) 1–10, doi:10.1016/s0022-2860(97)00291-3.
[42] S.R. Salman, F.S. Kamounah, Tautomerism in 1-hydroxy-2-naphthaldehyde Schiff bases: calculation of tautomeric isomers using carbon-13 NMR, Spectroscopy 17 (4) (2003) 747–752 iu, doi:10.1155/2003/531813.
[43] M. Ziółek, K. Filipczak, A. Maciejewski, Spectroscopic and photophysical properties of salicylaldehyde azine (SAA) as a photochromic Schiff base suitable for heterogeneous studies, Chem. Phys. Lett. 464 (4–6) (2008) 181–186, doi:10.1016/j.cplett.2008.09.030.
[44] D. Gürbüz, A. Cinarli, A. Tavman, A.S. Birteksz, Spectral characterization and antimicrobial activity of some Schiff bases derived from 4-Methyl-2-aminophenol, Chin. J. Chem. 30 (4) (2012) 970–978, doi:10.1002/cjoc.201100237.
[45] Ç. Albayrak Kaştaş, G. Kaştaş, A. Güder, M. Gür, H. Muğlu, O. Büyükgüngör, Investigation of two o -hydroxy Schiff bases in terms of prototropy and radical scavenging activity, J. Mol. Struct. 1130 (2017) 623–632, doi:10.1016/j.molstruc.2016.11.023.
[46] M. Juribašić, N. Bregović, V. Stilinović, V. Tomišić, M. Cindrić, P. Šket, K. žarević, Supramolecular stabilization of metastable tautomers in solution and the solid state, Chem. Eur. J. 20 (52) (2014) 17333–17345, doi:10.1002/chem.201403543.
[47] H. Tavakol, F. Keshavarzipour, A DFT study of inter- and intramolecular proton transfer in 2-selenobarbituric acid tautomers, Struct. Chem. 26 (2015) 1049–1057, doi:10.1007/s11224-015-0567-y.
[48] N. Darla, S. Sitha, Reaction between NH3 (X1A1) and CO (X1Σ+): a computational insight into the reaction mechanism of formamide (H2N-CHO) formation, J. Phys. Chem. A. 123 (2019) 8921–8931, doi:10.1021/acs.jpca.9b07255.
[49] Y. Yang, Y. Ma, Y. Zhao, Y. Zhao, Y. Li, Theoretical investigation of the reaction mechanism of photodeamination induced by excited-state intramolecular proton transfer of cresol derivatives, J. Phys. Chem. A 122 (2018) 1011–1018, doi:10.1021/acs.jpca.7b11571.
[50] Y. Li, X. Bai, R. Liang, X. Zhang, Y.H. Nguyen, B. VanVeller, L. Du, D.L. Phillips, Investigation of a series of 2-(2'-hydroxyaryl)benzazole derivatives: photophysical properties, excited-state intramolecular proton-transfer reactions, and observation of long-lived triplet excited states, J. Phys. Chem. B 125 (2021) 12981–12989, doi:10.1021/acs.jpcb.1c05798.
[51] S. Grimme, Semiempirical GGA-type density functional constructed with a long-range dispersion correction, J. Comput. Chem. 27 (2006) 1787–1799, doi:10.1002/jcc.20495.
[52] Y.S. Lin, G.D. Li, S.P. Mao, J.D. Chai, Long-range corrected hybrid density functionals with improved dispersion corrections, J. Chem. Theory Comput. 9 (2013) 263–272, doi:10.1021/ct300715s.
[53] A.E. Reed, R.B. Weinstock, F. Weinhold, Natural population analysis, J. Chem. Phys. 83 (1985) 735–746, doi:10.1063/1.449486.
[54] I. Brandao, T.L. Fonseca, L.R. Franco, H.C. Georg, M.A. Castro, Density functional theory investigation of the second hyperpolarizability of the phenol blue in solution, Chem. Phys. Lett. 796 (2022) 139549, doi:10.1016/j.cplett.2022.139549.
[55] L. Lescos, S.P. Sitkiewicz, P. Beaujean, M. Blanchard-Desce, B. Champagne, E. Matito, F. Castet, Performance of DFT functionals for calculating the second-order nonlinear optical properties of dipolar merocyanines, Phys. Chem. Chem. Phys. 22 (2020) 16579–16594, doi:10.1039/D0CP02992K.
[56] M. de Wergifosse, B. Champagne, Electron correlation effects on the first hyperpolarizability of push–pull π-conjugated systems, J. Chem. Phys. 134 (2011) 74113, doi:10.1063/1.3549814.
[57] G. Maroulis, On the electric dipole (hyper)polarizability of Difluorodiacetylene (F-C=C-C=C-F), Comput. Lett 2 (2006) 15–19, doi:10.1163/157404006777491936.
[58] P. Karamanis, G. Maroulis, An ab initio study of CX3-substitution (X = H, F, Cl, Br, I) effects on the static electric polarizability and hyperpolarizability of diacetylene, J. Phys. Org. Chem. 24 (2011) 588–599, doi:10.1002/poc.1797.
[59] A. Avramopoulos, L. Serrano-Andrés, J. Li, H. Reis, M.G. Papadopoulos, Linear and nonlinear optical properties of some organoxenon derivatives, J. Chem. Phys. 127 (21) (2007) 214102.
[60] A. Thomas, P.S. Patil, B. Siddlingeshwar, S.R. Manohara, N.B. Gummagol, G. Krishna Chaitanya, E M.Kirilova, Nonlinear optical properties of benzanthrone derivatives with N'-methylpiperazin-1-yl and N'-phenylpiperazin-1-yl substituents: experimental and quantum chemical study, Opt. Laser Technol. 156 (108616) (2022) 108616, doi:10.1016/j.optlastec.2022.108616.
[61] S. Jana, S. Dalapati, N. Guchhait, Proton transfer assisted charge transfer phenomena in photochromic Schiff bases and effect of –NEt2 groups to the Anil Schiff bases, J. Phys. Chem. A 116 (45) (2012) 10948–10958, doi:10.1021/jp3079698.
[62] L. McDonald, J. Wang, N. Alexander, H. Li, T. Liu, Y. Pang, Origin of water-induced fluorescence turn-on from a Schiff base compound: AIE or H-bonding promoted ESIPT? J. Phys. Chem. B 120 (4) (2016) 766–772, doi:10.1021/acs.jpcb.5b10909.
[63] W.J. Wang, L. Hao, C.Y. Chen, Q.M. Qiu, K. Wang, J.B. Song, H. Li, Red-shift in fluorescence emission of D–A type asymmetrical Zn(ii) complexes by extending the π–π stacking interaction, RSC Adv. 7 (33) (2017) 20488–20493, doi:10.1039/c7ra01135k.